

Fabrication of topological insulator devices

Oliver Breunig¹ & Yoichi Ando^{1*}

¹*Physics Institute II, University of Cologne, Zùlpicher Str. 77, 50937 Köln, Germany*

**Corresponding author. email: ando@ph2.uni-koeln.de*

Abstract

Topological insulators are expected to be a promising platform for exciting quantum phenomena, whose experimental realizations require sophisticated devices. However, topological-insulator materials are generally more delicate than conventional semiconductor materials and the fabrication of high-quality devices has been a challenge. In this Expert Recommendation, we discuss the nature of this challenge and present useful tips for successful device fabrications, taking superconducting and ferromagnetic devices as concrete examples. We also recommend some promising future directions.

1 Introduction

After more than 10 years of research, the understanding of topological insulator (TI) materials¹ has been well advanced. The next step is to use them as a platform for devices to realize novel and useful topological phenomena, such as emergence of chiral Majorana fermions^{2,3}, topological qubits using Majorana zero-modes^{4,5}, or topological magnetoelectric effects⁶ in the axion insulator

state⁷. Also, mesoscopic physics of the topological states of matter is a rich realm⁸, but it has been largely left unexplored. Hence, TI devices provide promising opportunities for new discoveries.

However, almost all known TI materials are much less robust against device fabrications compared to typical semiconductor materials such as Si or GaAs. Also, the functionally active part of TIs is the surface states and the bulk conduction should be suppressed as much as possible. These circumstances make it important to accumulate fabrication know-hows specifically developed for TI devices. Already, various kinds of TI devices have been fabricated, allowing for observations of interesting phenomena peculiar to TIs^{2,9-15}. This Expert Recommendation is aimed at helping researchers to save their efforts by providing some key know-hows and giving the general audience a concise view on the interesting technical challenges that TI materials pose before being used for ambitious purposes.

In the following, we provide concrete device fabrication tips and describe the techniques that are relevant to TI devices, focusing on tetradymite TI materials¹. In particular, we discuss superconducting devices in detail, because they are currently the most active and interesting areas of TI device research. We expect that our recommendation will promote high-quality experiments on TI devices in future.

2 Motivation for TI devices

TIs are characterized by a nontrivial Z_2 topology of their bulk electronic wave functions, which leads to the appearance of topologically-protected Dirac surface states¹. The most important prop-

erty of the topological surface states is the spin-momentum locking, which lifts the spin degeneracy and dictates the spin orientation depending on the momentum k . In fact, this property makes TIs a promising platform for topological superconductivity or spintronic devices.

In this article, we will discuss TI-based superconducting devices in detail, but there are of course many other types of TI-based devices that are promising for the research of topological phenomena and their applications. One interesting avenue would be to utilize a quantum anomalous Hall insulator (QAHI), i.e., ferromagnetic topological insulators whose chemical potential is tuned into the magnetic exchange gap opened at the Dirac point. By orienting the magnetization of the top and bottom surfaces in opposite directions, one can realize an axion insulator⁷, in which charge polarization will induce bulk magnetization with the proportionality coefficient equal to fine structure constant α ($= e^2/\hbar c$); this is called topological magnetoelectric effect⁶. Also, by inducing superconductivity in a QAHI via proximity effect, one can generate chiral Majorana fermions at the edges. There are already experimental works along this line^{2,3}, but the generation of chiral Majorana fermions remains controversial³.

Another fruitful direction is TI-based spintronic devices. While the current-induced spin-polarization on the TI surface has been demonstrated¹⁶, the efficiency of the spin generation in the diffusive transport regime is inherently low¹⁷. On the other hand, in the ballistic transport regime, the spin-momentum locking means that a 100% spin polarization is expected in theory. Hence, TI-based nanodevices to pursue this avenue would be very useful. Yet another interesting direction is TI-based nanodevices to address mesoscopic physics of TIs. In this regard, the size quantization

in TI nanowires leads to a gap opening and the formation of spin-degenerate subbands^{8,18}, but the spin degeneracy of the subbands (as well as the gap at the Dirac point) can be manipulated by a magnetic flux threading the nanowire axis. The tunability of the spin degeneracy would lead to a novel mesoscopic effect, which can only be detected in nanodevices.

3 Challenges of handling TIs

There are three main challenges when fabricating devices made out of TIs — preserving the insulating bulk, protecting the surface states, and being able to control the surface states by tuning the Fermi level relative to the Dirac point.

Preserving the insulating bulk Devices based on TIs are most exciting due to the peculiar properties of their conducting surface states. Their contribution can be enhanced not only by using thin films and exfoliated flakes to achieve a large surface-to-bulk ratio, but also by tuning the materials growth such that the chemical potential lies within the bulk band gap. Given the term of “topological *insulator*”, the insulation of the bulk may seem like a natural property of these materials. However, due to naturally-occurring self-doping, most of the TI compounds such as the binary tetradymite Bi_2Se_3 , Bi_2Te_3 , or Sb_2Te_3 conduct in their bulk. Nevertheless, the experimental challenge to realize a truly insulating bulk has been overcome by “compensation” of dopants, which can be achieved, for example, in the solid-solution of tetradymite compounds having opposite types of naturally-occurring carriers¹. Two widely-used materials belong to this class — $(\text{Bi}_x\text{Sb}_{1-x})_2\text{Te}_3$ (hereafter called BST)¹⁹ for thin films and $\text{Bi}_{2-x}\text{Sb}_x\text{Te}_{3-y}\text{Se}_y$ (called BSTS) for

bulk crystals²⁰.

Upon device fabrication, it is crucial to retain the insulation of the bulk. Since a major benefit of devices is to have the possibility of gate-tuning the chemical potential, the large density of states coming from conducting bulk would prevent any efficient tuning due to screening, spoiling this benefit. This requires special care that the chemical composition of the TI to be kept intact by not heating the sample too much during the resist baking or depositions of metals and dielectrics; in the cases of BST films and BSTS flakes, the recommended maximum temperature is 120°C.

Protecting the surface states It is important to note that the surface of BST and BSTS are oxidized in ambient atmosphere. This oxidation causes electron doping, but besides that, there has been no evidence that oxidation degrades the electron mobility in the surface states²¹ — most likely, the surface states just migrate beneath the oxide layer without experiencing enhanced scattering. On the other hand, the oxide layer poses a problem upon taking ohmic contacts or inducing superconductivity through a metal/superconductor deposited on the surface. The oxidation can be avoided by capping the TI surface with, for example, Te or Al₂O₃. To remove the oxide layer, wet etching (described later) is recommended over dry etching.

Also, not damaging the surface during the device fabrication is important for keeping the mobility of the surface states; when *in-situ* cleaning of the surface using Ar plasma is performed before deposition of metals, the plasma power should be kept to a minimum.

Controlling the surface states For electrostatic gating, the thickness of the film or flake is decisive. It should be thin enough to sufficiently reduce residual bulk conductivity and to allow for microfabrication — typical resist for lithography impose an upper limit of roughly 100 nm on the range of useful TI thicknesses. Yet, even down to about 20 nm a single gate electrode can only tune the electron density of only one of the two (top or bottom) surfaces effectively. Additionally, the interface-dependent band bending effects introduce asymmetry between the two surfaces. Hence, top and bottom surfaces need to be considered as two distinct channels whose chemical potential and thus the conductance differ. To evaluate the contributions of the top and bottom surfaces in the total conductance, a two-band analysis of the magnetic-field dependence in the Hall resistance, $R_{yx}(H)$, from a device such as shown in Fig. 1a, is useful¹.

The independence of top and bottom surface channels mentioned above makes it difficult to attain the unique situation where the chemical potential is tuned exactly at the Dirac point, by gating the TI from either the top or the bottom side alone. To achieve full tuning to the Dirac point^{12,22,23}, both sides of the TI need to be gated simultaneously, which is called “dual gating”. Nevertheless, for thicknesses below about 20 nm another route opens up. In this case, the two surfaces are close enough such that both of them can be tuned reasonably well by gating from just one side²⁴. Although it is no problem to growth films thinner than ~ 20 nm by MBE, for flakes, the challenge lies in optimizing the exfoliation technique to obtain thin-enough flakes with acceptable yield and in identifying them by their different optical properties. Note that, even for films and flakes thinner than ~ 20 nm, the chemical potential may have an offset between top and bottom surfaces, albeit being simultaneously tunable.

4 Fabricating devices (see Box 1 for clean-room equipment recommendation)

Choosing the material Bulk-insulating BST thin films can be grown with molecular beam epitaxy (MBE) by subtle tuning of flux ratios and growth temperatures¹⁹. Because the growth proceeds in the van-der-Waals epitaxy mode¹, the lattice-constant matching of the substrate is not required for the epitaxy. While silicon wafers are compatible with well-established industry tools and allow for epitaxial growth of BST¹⁵, sapphire (Al_2O_3) wafers tend to give better film qualities²⁴. The substrate cleaning is crucial for a successful epitaxy; in the case of sapphire wafers, for example, a combination of thorough washing, plasma cleaning, and vacuum annealing at 950°C gives sufficiently clean surface.

Due to the layered structure and weak van-der-Waals bonds of 3D TIs of the tetradymite family, exfoliation of melt-grown bulk crystals of BSTS into thin flakes is another route to obtaining high-quality bulk-insulating TIs ready for device fabrication. A major advantage of flakes over thin films is the flexibility in the choice of substrates to exfoliate on. Conducting substrates coated with an insulating dielectric, e.g. doped Si coated with SiO_2 , can be used for simple realization of a gate.

Surface protection To preserve the transport properties of TIs upon device fabrication, some special care needs to be taken. First, aging due to surface oxidation can degrade the device performance, through doping and the migration of the surface states deeper in to the sample. The oxidation dynamics depends on the chemical composition of the TI material and its surface morphology^{25,26}. For strongly-terraced MBE thin films, surface oxidation is more relevant than for

exfoliated flakes that are almost atomically-flat. Typically, at ambient conditions, sizable oxidation occurs within minutes to hours, and thus, air exposure of the device under fabrication needs to be minimized. Another, more practical route is to cap films *in-situ* or right after the growth with minimal air exposure. As a capping layer for BST, tellurium layer grown *in-situ* in a MBE chamber, or Al₂O₃ layer grown *in-situ* by electron-beam evaporation/sputtering or *ex-situ* with atomic-layer deposition (ALD), have proven successful^{24,27,28}. Depositing a thin layer of aluminum and letting it oxidize to form AlO_x is less suitable, as aluminum alloys with TIs²⁹. However, this process can be useful for capping other metals or superconductors in order to protect those from oxidation.

Lithography Since BST and BSTS are chemically not very stable, for the fabrication of their devices, established semiconductor-based fabrication processes need to be reconsidered, starting with the choice of process chemicals. Solvents like acetone and IPA can be used safely and do not degrade the TI's properties. However, TMAH-based developers for photo-lithography considerably etch TI films on a nm/min scale. Thus, when working with very thin films or flakes, the development time must be tuned precisely, or preferably electron beam lithography had better be employed. For thicker films the finite etch rate, in contrast, can be beneficial and reduce the contact resistance via the removal of a native oxide layer during the development. Further, TMAH-based developers etch Al₂O₃ at about 10 nm/min (2.38% TMAH) which needs to be taken into account when fabricating a gate electrode with Al₂O₃ dielectric or when using sapphire substrates. For commonly used electron beam resists and developers, no such incompatibility arises.

For device fabrications based on exfoliated flakes, it is extremely helpful to use prefabricated

substrates of about $10 \times 10\text{-mm}^2$ size patterned with a closely spaced array of markers for coordination in lithography (see Fig. 1b). The thickness of exfoliated flakes can be judged most efficiently by optical microscopy based on the shade of the flake in the bright field and the contrast of its edge in the dark field (see Fig. 1a) in the crucial thickness range of 5–30 nm.

Electrical contacts For making electrical contacts it is mandatory to remove any kind of capping layer right before metallization. Here, plasma etching, even if performed *in-situ*, is not a preferred option, because the etch rate of the tetradymite TIs even at low ion energies is large compared to the capping materials. Thus, even a slight over-etch of the capping layer can quickly remove the whole TI underneath. Larger selectivity is achieved by wet etching, for example, by using aluminum etchant (Type D, Transene) for Al_2O_3 removal. It is essential to avoid etchant residues by thoroughly washing afterwards. Due to the potentially non-trivial microfluidics of sub- μm features during the etch, an in-detail analysis and optimization of the capping-layer removal should be performed. Apparently, oxidation occurs again right after removing the capping layer in the crucial interfacial areas. Therefore, the transfer to the vacuum chamber of the deposition system either needs to be performed rapidly or a flow box is used together with a suitable vacuum-tight transfer box and/or a portable nitrogen bag.

Making electrostatic gates As discussed above, full gate control can only be achieved via dual gating. For thin films this requires transferring the film from the growth substrate to a suitable fabrication substrate, e.g. a doped-Si substrate coated with SiO_2 , via a detaching technique²² (see Fig. 1c). The film quality of the gate dielectric decides the later device performance in terms of

hysteresis due to trap states, pinning of the chemical potential by localized states, leakage because of pinholes, and premature breakdown due to defects. In this sense, oxides grown in a dry process are preferable and typically used for the back gate. For TI devices, the growth of the dielectric layer needs to be performed without heating the TI material too much, even though a high-quality gate dielectric often requires a high-temperature growth; in this regard, among the suitable materials and techniques for the fabrication of the top gate are silicon nitride grown by hot-wire CVD²⁴, aluminum oxide grown by ALD³⁰, and flakes of h-BN transferred onto TI flakes^{23,31}.

5 Interfacing TIs with superconductors

The devices to elucidate the emergence of topological superconductivity and associated Majorana bound states (MBS) in hybrid structures of a superconductor (SC) and a TI^{32,33} are one of the most interesting classes of TI devices. However, the fabrication of such devices is very challenging due to the difficulty in preparing the necessarily clean interfaces with high transparency between the two materials (see Fig. 2 for exemplary devices). In the following, we describe specific know-hows for such TI/SC hybrid devices (see Box 2 for characterization tips).

Needless to say, oxidation and excessive heating must be avoided to preserve the TI's properties, but in addition, the TI surface should be free from residual oxides and adsorbates when a SC layer is deposited. Successive *in-situ* deposition of a SC onto a freshly-grown TI thin film is a possibility²⁹, but an epitaxial growth of a SC compatible with post-fabrication of nano-devices has not been achieved. In an *ex-situ* process, interface cleaning can be performed by gentle (reactive)

ion etching and dilute acid treatment³⁴. In addition, *in-situ* ion milling at low energies ($\lesssim 90$ eV) can help to prepare pristine surfaces. Yet, the ion energy and milling time should be tuned carefully, as detrimental effects induced by excessive milling may dominate and affect the mobility of the surface carriers of interest. Also, the usefulness of *in-situ* cleaning needs to be assessed for the particular TI material and the individual instrument at hand. TI thin films usually has a high density of step edges on their surface, such that the microscopies of the ion-beam interaction is different from that on exfoliated flakes having a much flatter surface.

Besides physically cleaning the interface, the choice of the proximitizing SC material and/or the adhesion-layer material is crucial for achieving a high interface transparency (see Table 1 for an overview). Not all common SC materials can be used directly on top of TI materials due to potential alloying with the TI. For example, among the popular SC materials, aluminum (Al) alloys with BST(S)²⁹. Thus, it is often necessary to first coat the TI with an adhesion layer which also acts as a diffusion barrier. Platinum and titanium are commonly used as adhesion layers. They mediate a good electrical contact together with superconducting Al or V, but also with normal metals such as Au. Typical thickness of the adhesion layer is in the range of about 5 nm, i.e. thick enough to be continuous and protective for the TI, but also thin enough not to hinder the superconducting proximity effect to reach the TI. Niobium provides good electrical contact even without any sticking layer and adheres very well. However, the adhesion to the TI can be even stronger than that of TI films to the substrate, which may lead to odd liftoff results.

Nanowires Nanowires of TIs represent the straightforward implementation of the fundamental concept to realize MBS³⁵. In such nanowires the Dirac surface states acquire a gap and split into subbands. With half-integer values of the flux quantum $(n + \frac{1}{2})h/e$ piercing the wire and in proximity to an *s*-wave superconductor, a topological 1D superconducting state can be realized irrespective of the location of the chemical potential¹⁸. Suitable nanowires can be obtained in various ways. The vapor-liquid-solid (VLS) growth yields TI nanowires in length of a few μm of consistent morphology (Fig. 3a) with relatively low instrumental efforts^{8,36}. Hydrothermal synthesis³⁷ or exfoliation of bulk crystals⁹ can also result in thin TI nanoribbons, although the yield in the latter case is extremely low and the regime of one-dimensional transport is achieved for very narrow ribbons only.

The approach of etching a continuous thin film into desired nanowires (or a network of them) promises virtually unlimited design freedom and well-controllable properties of the obtained nanowires, while requiring highly tuned processes and sophisticated machinery. Nanostructures with carrier mobilities retained from the pristine film can be obtained by a combination of dry ion etching and wet etching with a 3:1 dilution of $\text{H}_2\text{O}_2:\text{H}_2\text{SO}_4$ (examples in Figs. 3b&1a). The “selective area growth” method (Fig. 3c) of pre patterning a substrate with a growth mask for subsequent epitaxy allows for complex device designs as well and can additionally be extended to employ *in-situ* deposition of superconductors by using suspended growth masks^{15,38}. Interfacing bulk-insulating TI nanowires with superconductors is an important immediate challenge.

6 Interfacing TIs with ferromagnets

Ferromagnets in contact with the TI surface offer two types of functionalities. One is to break time reversal symmetry in the TI surface states through “magnetic proximity effect” and to open up a magnetic exchange gap at the Dirac point. The other is spintronic functionalities, either to detect the spin polarization on the TI surface or even to present magnetization switching due the spin-orbit torque exerted from the TI. Insulating ferromagnets are used for the magnetic proximity effect, while metallic ferromagnets are used for spintronic devices.

For the magnetic proximity effect, the ferromagnetic insulator EuS grown on Bi_2Se_3 has been used for devices to detect chiral currents at magnetic domain boundaries³⁹ or to induce ferromagnetism in the TI surface at room temperature⁴⁰. Also, magnetic proximity effect is a cleaner way to induce ferromagnetism in the TI surface states than magnetic doping to maintain a high carrier mobility, and the quantum anomalous Hall effect has recently been achieved by interfacing the ferromagnetic insulator $\text{Zn}_{1-x}\text{Cr}_x\text{Te}$ to BST⁴¹. For efficient magnetic proximity effects, using the MBE technique to realize epitaxial interface is crucial^{40,41}.

In spintronic devices based on TIs, ferromagnetic metals have been used as a spin-voltage detector to probe the current-induced spin polarization in the spin-momentum locked surface states^{16,17}. Thermally-evapolated Permalloy is commonly used for this purpose. For the spin-voltage detection, non-Ohmic, high resistance contact is preferred to compensate for the impedance mismatch at the interface, and a tunnel barrier is typically inserted in between the TI and the ferromagnet to enhance the spin voltage. In terms of fabrication, deposition of the tunnel barrier

material (typically Al_2O_3 or MgO) requires special care, such as preparing a pristine TI surface, avoiding pinholes, and achieving reproducible thickness control in order to tune the contact resistance, which depends exponentially on the tunnel barrier thickness.

The current-induced spin polarization can be used for switching the magnetization of a ferromagnetic metal in direct contact with the TI surface. Such devices use spin-orbit torque, which requires a good metallic contact. The first demonstration of the switching operation was performed in an epitaxially-grown bilayer of BST and ferromagnetic Cr-doped BST⁴². A very efficient spin-orbit torque switching has been reported⁴³ for a device based on $\text{Bi}_{0.9}\text{Sb}_{0.1}$ and MnGa.

7 Recommendations

For devices to exploit the peculiar surface-state properties of TIs, usage of bulk-insulating materials such as MBE-grown BST thin films or exfoliated BSTS flakes are recommended. To preserve the surface-state mobility as well as the bulk-insulating nature, too much heating and dry etching should be avoided, and usages of capping layer and wet etching are recommended. For electrostatic gating to control the chemical potential, one should keep in mind that top and bottom surfaces form independent conduction channels, and dual gating is recommended for a full control of the chemical potential.

The technologies to realize clean interfaces between TIs and other materials are not sufficiently developed. *In-situ* epitaxial growth of superconductors and ferromagnetic insulators are desirable for better superconducting- and magnetic-proximity effects. In this respect, more efforts

had better be focused on the realization of epitaxial interfaces for superconducting and QAHI devices. Furthermore, epitaxially-grown heterostructure of a TI and a ferromagnetic insulator can be a platform to realize new topological states of matter⁴⁴, so the combination of heterostructure growth and device fabrication will have a particularly bright prospect.

Acknowledgements: We thank J. Feng, M. Rössler, D. Fan, L. Dang, F. Munning, G. Lippertz and A. Taskin for providing device pictures, and D. Grützmacher, P. Schüffelgen, and F. Yang for useful discussions. This work has received funding from the European Research Council (ERC) under the European Union’s Horizon 2020 research and innovation programme (grant agreement No 741121) and was also funded by the Deutsche Forschungsgemeinschaft (DFG, German Research Foundation) under CRC 1238 - 277146847 (Subprojects B01) and AN 1004/4-1 - 398945897, as well as under Germany’s Excellence Strategy - Cluster of Excellence Matter and Light for Quantum Computing (ML4Q) EXC 2004/1 - 390534769.

Author contributions: Y.A. conceived the article with input from O.B. O.B. and Y.A. wrote the manuscript.

Competing Interests: The authors declare no competing interests.

8 Box 1: Equipment needed for TI device fabrication

- **clean room infrastructure:** To date, TI devices are typically fabricated in small batches as prototypes, such that the functional device parts cover only a few μm^2 on the substrates.

Thus, the requirements on the clean room class are fairly low. Nevertheless, yellow lightning is required to enable optical lithography processes. A wet bench or fume hood is needed for working safely with solvents, developers, and acids. For high-resolution lithography, vibration-isolation and/or reinforced floor plates may be required for the installation of an electron-beam writer. The room temperature needs to be stable within a few °C as some development and etching processes strongly depend on temperature.

- **lithography:** optical lithography (with mask aligner or maskless laser writer) for prepattern- ing wafers with markers and pads; electron-beam lithography with good overlay accuracy, which requires laser interferometry stage.
- **analysis:** scanning electron microscope; atomic force microscope; high-grade optical mi- croscope (laser confocal microscope) with dark-field option, camera, and yellow-light filter.
- **deposition** (necessary machines depend on the choice of metals and superconductors): UHV sputtering system with *in-situ* low-energy (< 100 eV) ion gun; electron-beam evaporator; thermal evaporator; atomic layer deposition (ALD) machine.
- **etching:** reactive ion etching (RIE) machine for dry etching and interface cleaning; hot plate with magnetic stirrer and water bath for wet etching.

9 Box 2: Analysis of TI/superconducting devices

The success of interfacing the TI with superconductors needs to be judged from the device char- acteristics, mostly by performing transport experiments in a dilution fridge. The contact resistance

can be a rough indication of the interface cleanliness. Typical contact resistivities of well-prepared contacts are of the order of $100 \Omega \mu\text{m}^2$ and should hardly depend on temperature. In-depth information can be gained from Josephson junctions, where two superconducting electrodes are placed on top of the TI with a small gap in between them, such that a SNS junction is formed through the TI in a planar geometry. When the TI material is bulk-insulating, the gap between the electrodes should be narrower than ~ 80 nm. The width of the superconducting leads should be kept small enough (shorter than the London penetration depth) such that Abrikosov vortices will not penetrate. Abrikosov vortices formed near the junction would alter the effective flux through the junction area and thus make it difficult to observe the Fraunhofer pattern in the magnetic-field dependence of the critical current I_c , which gives insight into the homogeneity of the SC/TI interface and serve as a proof of proximity-induced superconductivity³⁴.

In addition to the Fraunhofer-pattern measurement, the I - V characteristics (Fig. 4) of the junction should be measured to perform the following analyses:

- (i) Comparison of the $I_c R_n$ product to the superconductor's bulk gap $\Delta_{\text{SC}} = 1.76 k_B T_c$
- (ii) Estimation of the induced superconducting gap Δ_{ind} by indexing the multiple Andreev reflections observed at $V_n = 2\Delta_{\text{ind}}/en$ in the resistive state^{45,46}, and compare it with Δ_{SC}
- (iii) Estimation of the transparency^{45,47} of the SC/TI interface from Δ_{ind} , excess current I_e , and the normal-state resistance R_n
- (iv) Extraction of the transparency between the proximitized TI underneath the SC electrodes and the pristine TI part in the junction gap from the temperature dependence of the critical current^{15,48}

The incentive to induce superconductivity in TIs comes from the possibility to generate MBS. Though indirect, one of the key expected features is a 4π -periodic relation of the current across the junction to the phase difference across it⁴⁹. It is reflected in the missing of Shapiro steps $V = nhf/2e$ with odd index n upon irradiating the junction by a microwave of frequency f , as observed in a few experiments^{10,50,51}, or in the appearance of the microwave radiation with half the Josephson frequency, $\frac{1}{2}f_J [= \frac{1}{2}(2eV_{dc}/h)]$, from the junction¹¹.

References:

1. Ando, Y. Topological insulator materials. *J. Phys. Soc. Jpn.* **82**, 102001 (2013).
2. He, Q. L. *et al.* Chiral Majorana fermion modes in a quantum anomalous Hall insulator–superconductor structure. *Science* **357**, 294–299 (2017).
3. Kayyalha, M. *et al.* Absence of evidence for chiral Majorana modes in quantum anomalous Hall-superconductor devices. *Science* **367**, 64–67 (2020).
4. Aguado, R. & Kouwenhoven, L. P. Majorana qubits for topological quantum computing. *Phys. Today* **73**, 44–50 (2020).
5. Manousakis, J., Altland, A., Bagrets, D., Egger, R. & Ando, Y. Majorana qubits in a topological insulator nanoribbon architecture. *Phys. Rev. B* **95**, 165424 (2017).
6. Qi, X.-L., Hughes, T. L. & Zhang, S.-C. Topological field theory of time-reversal invariant insulators. *Phys. Rev. B* **78**, 195424 (2008).

7. Mogi, M. *et al.* A magnetic heterostructure of topological insulators as a candidate for an axion insulator. *Nat. Mater.* **16**, 516–521 (2017).
8. Munning, F. *et al.* Quantum confinement of the Dirac surface states in topological-insulator nanowires. *arXiv e-prints* arXiv:1910.07863 (2019).
9. Cho, S. *et al.* Aharonov-Bohm oscillations in a quasi-ballistic three-dimensional topological insulator nanowire. *Nat. Commun.* **6**, 7634 (2015).
10. Wiedenmann, J. *et al.* 4π -periodic Josephson supercurrent in HgTe-based topological Josephson junctions. *Nat. Commun.* **7**, 10303 (2016).
11. Deacon, R. S. *et al.* Josephson radiation from gapless Andreev bound states in HgTe-based topological junctions. *Phys. Rev. X* **7**, 021011 (2017).
12. Taskin, A. A. *et al.* Planar Hall effect from the surface of topological insulators. *Nat. Commun.* **8**, 1340 (2017).
13. Yasuda, K. *et al.* Quantized chiral edge conduction on domain walls of a magnetic topological insulator. *Science* **358**, 1311–1314 (2017).
14. Chen, A. Q. *et al.* Finite momentum Cooper pairing in three-dimensional topological insulator Josephson junctions. *Nat. Commun.* **9**, 3478 (2018).
15. Schüffelgen, P. *et al.* Selective area growth and stencil lithography for in situ fabricated quantum devices. *Nat. Nanotech.* **14**, 825–831 (2019).

16. Li, C. H. *et al.* Electrical detection of charge-current-induced spin polarization due to spin-momentum locking in Bi_2Se_3 . *Nat. Nanotechnol.* **9**, 218–24 (2014).
17. Yang, F. *et al.* Switching of charge-current-induced spin polarization in the topological insulator BiSbTeSe_2 . *Phys. Rev. B* **94**, 075304 (2016).
18. Cook, A. & Franz, M. Majorana fermions in a topological-insulator nanowire proximity-coupled to an s-wave superconductor. *Phys. Rev. B* **84**, 201105 (2011).
19. Zhang, J. *et al.* Band structure engineering in $(\text{Bi}_{1-x}\text{Sb}_x)_2\text{Te}_3$ ternary topological insulators. *Nat. Commun.* **2**, 574 (2011).
20. Ren, Z., Taskin, A. A., Sasaki, S., Segawa, K. & Ando, Y. Optimizing $\text{Bi}_{2-x}\text{Sb}_x\text{Te}_{3-y}\text{Se}_y$ solid solutions to approach the intrinsic topological insulator regime. *Phys. Rev. B* **84**, 165311 (2011).
21. Taskin, A. A., Ren, Z., Sasaki, S., Segawa, K. & Ando, Y. Observation of Dirac holes and electrons in a topological insulator. *Phys. Rev. Lett.* **107**, 016801 (2011).
22. Yang, F. *et al.* Dual-gated topological insulator thin-film device for efficient Fermi-level tuning. *ACS Nano* **9**, 4050–4055 (2015).
23. Wang, J. *et al.* Two-dimensional-Dirac surface states and bulk gap probed via quantum capacitance in a three-dimensional topological insulator. *Nano Lett.* **20**, 8493–8499 (2020).
24. Yang, F. *et al.* Top gating of epitaxial $(\text{Bi}_{1-x}\text{Sb}_x)_2\text{Te}_3$ topological insulator thin films. *Appl. Phys. Lett.* **104**, 161614 (2014).

25. Volykhov, A. A. *et al.* Rapid surface oxidation of Sb_2Te_3 as indication for a universal trend in the chemical reactivity of tetradymite topological insulators. *Chem. Mater* **28**, 8916–8923 (2016).
26. Volykhov, A. A. *et al.* Can surface reactivity of mixed crystals be predicted from their counterparts? A case study of $(\text{Bi}_{1-x}\text{Sb}_x)_2\text{Te}_3$ topological insulators. *J. Mater. Chem. C* **6**, 8941–8949 (2018).
27. Hofer, K., Becker, C., Wirth, S. & Hao Tjeng, L. Protective capping of topological surface states of intrinsically insulating Bi_2Te_3 . *AIP Adv.* **5**, 097139 (2015).
28. Steinberg, H., Laloë, J.-B., Fatemi, V., Moodera, J. S. & Jarillo-Herrero, P. Electrically tunable surface-to-bulk coherent coupling in topological insulator thin films. *Phys. Rev. B* **84**, 233101 (2011).
29. Schüffelgen, P. *et al.* Stencil lithography of superconducting contacts on MBE-grown topological insulator thin films. *J. Cryst. Growth* **477**, 183 – 187 (2017).
30. Checkelsky, J. G. *et al.* Trajectory of the anomalous Hall effect towards the quantized state in a ferromagnetic topological insulator. *Nat. Phys.* **10**, 731–736 (2014).
31. Fatemi, V. *et al.* Electrostatic coupling between two surfaces of a topological insulator nanodevice. *Phys. Rev. Lett.* **113**, 206801 (2014).
32. Fu, L. & Kane, C. L. Superconducting proximity effect and Majorana fermions at the surface of a topological insulator. *Phys. Rev. Lett.* **100**, 096407 (2008).

33. Sato, M. & Ando, Y. Topological superconductors: a review. *Rep. Prog. Phys.* **80**, 076501 (2017).
34. Ghatak, S. *et al.* Anomalous Fraunhofer patterns in gated Josephson junctions based on the bulk-insulating topological insulator BiSbTeSe₂. *Nano Lett.* **18**, 5124–5131 (2018).
35. Kitaev, A. Y. Unpaired Majorana fermions in quantum wires. *Phys. Usp.* **44**, 131–136 (2001).
36. Peng, H. *et al.* Aharonov-Bohm interference in topological insulator nanoribbons. *Nat. Mater.* **9**, 225–229 (2010).
37. Xiu, F. *et al.* Manipulating surface states in topological insulator nanoribbons. *Nat. Nanotechnol.* **6**, 216–221 (2011).
38. Rosenbach, D. *et al.* Quantum transport in topological surface states of selectively grown Bi₂Te₃ nanoribbons. *Adv. Electron. Mater.* **6**, 2000205 (2020).
39. Wang, Y. H. *et al.* Observation of chiral currents at the magnetic domain boundary of a topological insulator. *Science* **349**, 948–952 (2015).
40. Katmis, F. *et al.* A high-temperature ferromagnetic topological insulating phase by proximity coupling. *Nature* **533**, 513–516 (2016).
41. Watanabe, R. *et al.* Quantum anomalous Hall effect driven by magnetic proximity coupling in all-telluride based heterostructure. *Appl. Phys. Lett.* **115**, 102403 (2019).
42. Fan, Y. *et al.* Magnetization switching through giant spin–orbit torque in a magnetically doped topological insulator heterostructure. *Nat. Mater.* **13**, 699–704.

43. Khang, N. H. D., Ueda, Y. & Hai, P. N. A conductive topological insulator with large spin Hall effect for ultralow power spin–orbit torque switching. *Nat. Mater.* **17**, 808–813 (2018).
44. Burkov, A. A. & Balents, L. Weyl semimetal in a topological insulator multilayer. *Phys. Rev. Lett.* **107**, 127205 (2011).
45. Octavio, M., Tinkham, M., Blonder, G. E. & Klapwijk, T. M. Subharmonic energy-gap structure in superconducting constrictions. *Phys. Rev. B* **27**, 6739–6746 (1983).
46. Xiang, J., Vidan, A., Tinkham, M., Westervelt, R. M. & Lieber, C. M. Ge/Si nanowire mesoscopic josephson junctions. *Nat. Nanotechnol.* **1**, 208–213 (2006).
47. Blonder, G. E., Tinkham, M. & Klapwijk, T. M. Transition from metallic to tunneling regimes in superconducting microconstrictions: Excess current, charge imbalance, and supercurrent conversion. *Phys. Rev. B* **25**, 4515–4532 (1982).
48. Galaktionov, A. V. & Zaikin, A. D. Quantum interference and supercurrent in multiple-barrier proximity structures. *Phys. Rev. B* **65**, 184507 (2002).
49. Fu, L. & Kane, C. L. Josephson current and noise at a superconductor/quantum-spin-Hall-insulator/superconductor junction. *Phys. Rev. B* **79**, 161408 (2009).
50. Bocquillon, E. *et al.* Gapless Andreev bound states in the quantum spin Hall insulator HgTe. *Nat. Nanotechnol.* **12**, 137–143 (2017).
51. Li, C. *et al.* 4π -periodic Andreev bound states in a Dirac semimetal. *Nat. Mater.* **17**, 875–880 (2018).

52. Kurter, C., Finck, A. D. K., Ghaemi, P., Hor, Y. S. & Van Harlingen, D. J. Dynamical gate-tunable supercurrents in topological Josephson junctions. *Phys. Rev. B* **90**, 014501 (2014).
53. Williams, J. R. *et al.* Unconventional Josephson effect in hybrid superconductor-topological insulator devices. *Phys. Rev. Lett.* **109**, 056803 (2012).
54. Bai, M. *et al.* Novel self-epitaxy for inducing superconductivity in the topological insulator $(\text{Bi}_{1-x}\text{Sb}_x)_2\text{Te}_3$. *Phys. Rev. Mat.* **4**, 094801 (2020).
55. Zhang, D. *et al.* Superconducting proximity effect and possible evidence for Pearl vortices in a candidate topological insulator. *Phys. Rev. B* **84**, 165120 (2011).
56. Bhattacharyya, B., Awana, V. P. S., Senguttuvan, T. D., Ojha, V. N. & Husale, S. Proximity-induced supercurrent through topological insulator based nanowires for quantum computation studies. *Sci. Rep.* **8**, 17237 (2018).
57. Yang, F. *et al.* Proximity-effect-induced superconducting phase in the topological insulator Bi_2Se_3 . *Phys. Rev. B* **86**, 134504 (2012).
58. Qu, F. *et al.* Strong superconducting proximity effect in $\text{Pb-Bi}_2\text{Te}_3$ hybrid structures. *Sci. Rep.* **2**, 339 (2012).
59. Trang, C. X. *et al.* Conversion of a conventional superconductor into a topological superconductor by topological proximity effect. *Nat. Commun.* **11**, 159 (2020).

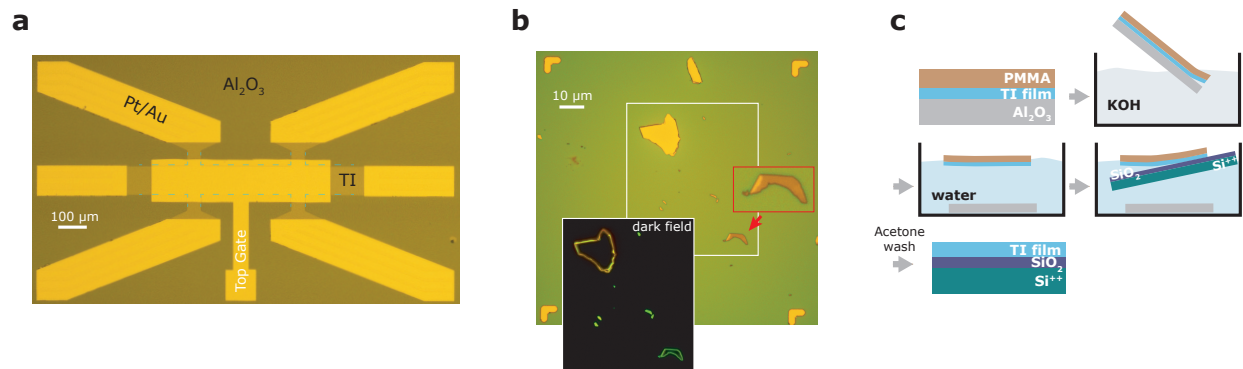


Figure 1: **Fabrication of TI devices.** **a**, Top-gated Hall bar device fabricated from a MBE-grown thin film. The dashed line indicates the edge of the etched Hall bar structure underneath the gate metal. **b**, Optical contrast of thin exfoliated flakes. The flake marked by a red arrow and shown in a magnified view (box framed red) is less than 20 nm thick and thus appears half-transparent. On its left edge the thickness is larger, indicated by a more bright color. In dark-field microscopy (inset) the edge of thin flakes is less apparent than that of thicker flakes. A dense array of prefabricated markers (corners of the image) is useful for precise alignment. **c**, Process of transferring a TI film from an Al₂O₃ growth substrate to a Si/SiO₂ substrate for dual-gating, following Ref. 22.

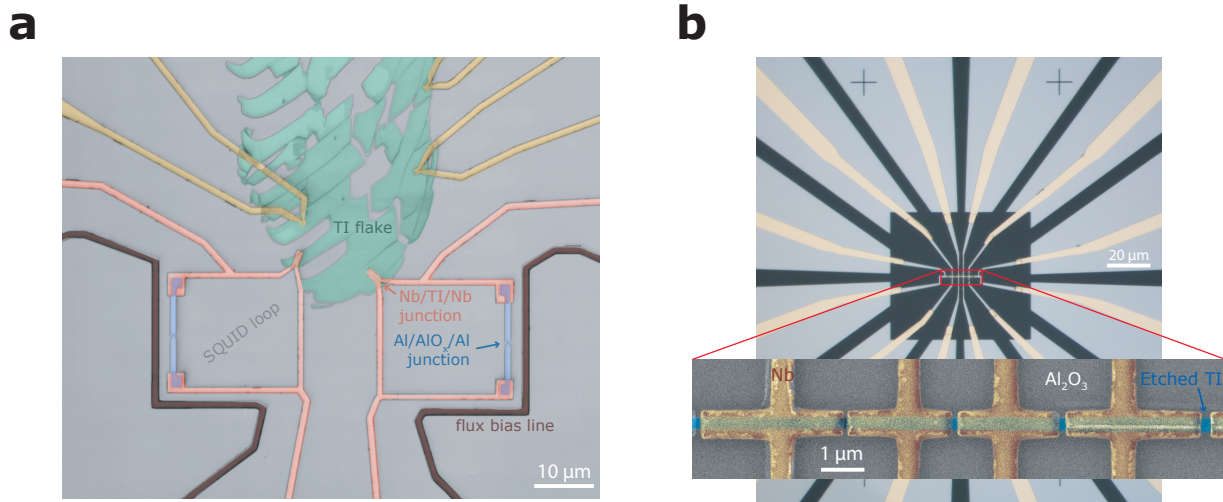


Figure 2: **TI-based Josephson junction devices.** **a**, False-color confocal laser micrograph of an asymmetric SQUID-device for investigating the current-phase-relation of a SC/TI/SC Josephson junction. The SQUID loop is formed by an Al/AIO_x/Al reference junction (blue) in parallel to a TI junction made from two close Nb leads (light red). A flux bias line (brown) is used to alter the flux through the loop. Auxiliary test junctions (yellow) are fabricated on top of the exfoliated flakes (green) in order to characterize the stand-alone SC/TI/SC junction. **b**, TI nanowire Josephson junction device fabricated by etching a MBE-grown thin film into a nanowire shape (optical image). The inset shows a close-up false-color scanning electron micrograph of the nanowire (blue shade) with differently spaced Nb leads (gold) on top.

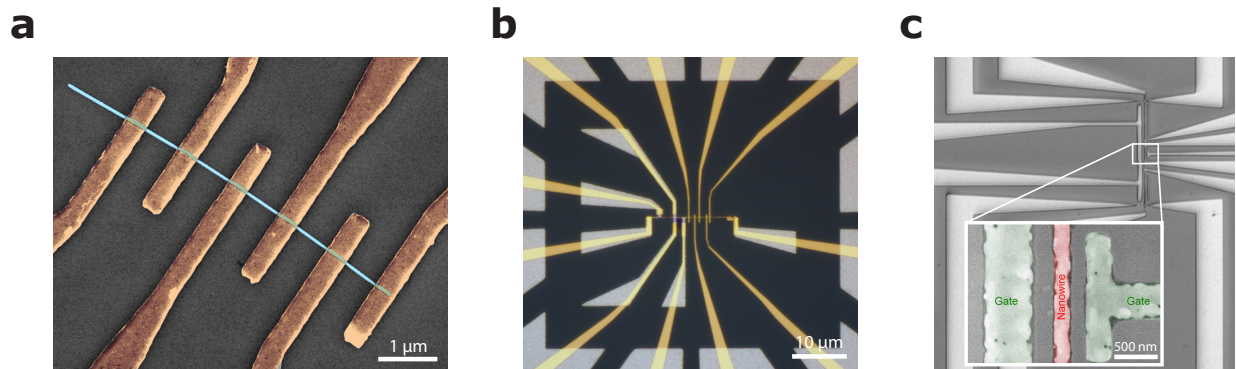


Figure 3: **Topological insulator nanowire devices.** **a**, False-color scanning electron micrograph of a device based on VLS-grown nanowire (colored light blue) for normal state transport measurements using electrodes (brown) made from 5 nm Pt + 40 nm Au. **b**, BST thin film (gray) etched into the shape of a nanowire. Contacts are either realized based on etched leads (5 left contacts & right-most contact) or by subsequent fabrication of Pt/Au finger contacts. **c**, nanowire device made by selective area growth. A BST film grows within the prepatterned trenches only (white areas of the main image). Multiple leads, but also gates (green areas in the false-color scanning electron micrograph shown in the inset), can be realized from BST in the same run.

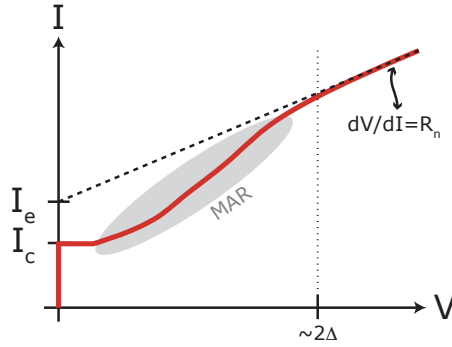


Figure 4: **Schematics of the IV -curve of a SC/TI/SC Josephson junction.** For currents larger than the critical current I_c , the measured IV -curve (red line) may contain signatures of multiple Andreev reflections (MAR) up to a voltage of 2Δ , where Δ is the induced superconducting gap. For voltages $V > 2\Delta$ a linear regime is entered, characterized by the normal state resistance R_n . Extrapolating this linear dependence yields the excess current I_e as the current-axis intercept.

SC material	adhesion layer	deposition method	comment
niobium (Nb)	–	UHV sputtering	great adhesion, high T_c ⁵²
aluminum (Al)	Ti, Pt	preferred: e-beam evaporation alternative: thermal evaporation	good transparency, considerable aging if not capped 34, 53
vanadium (V)	Ti	e-beam evaporation	good transparency, tricky liftoff
PdTe ₂	–	HV sputtering of Pd	self-formed upon deposition ⁵⁴
tungsten (W)	–	FIB	difficult to deposit ^{55, 56}
lead (Pb)	–	thermal evaporation	unpopular material for microfabrication ^{57, 58} , topological proximity effect ⁵⁹

Table 1: **Proximitizing superconductors.** Achieving a strong proximity effect requires well-tuned process parameters. Both the critical temperature/field and the morphology should be checked using plain films first.